ACS Chemical Neuroscience

pubs.acs.org/chemneuro Research Article

Curcumin and Homotaurine Suppress Amyloid-β_{25-35} Aggregation in Synthetic Brain Membranes

Xingyuan Zou, Sebastian Himbert, Alix Dujardin, Janos Juhasz, Samantha Ros, Harald D. H. Stöver, and Maikel C. Rheinstädter*

Cite This: *ACS Chem. Neurosci.* 2021, 12, 1395−1405 Read Online

ACCESS | Metrics & More | Article Recommendations

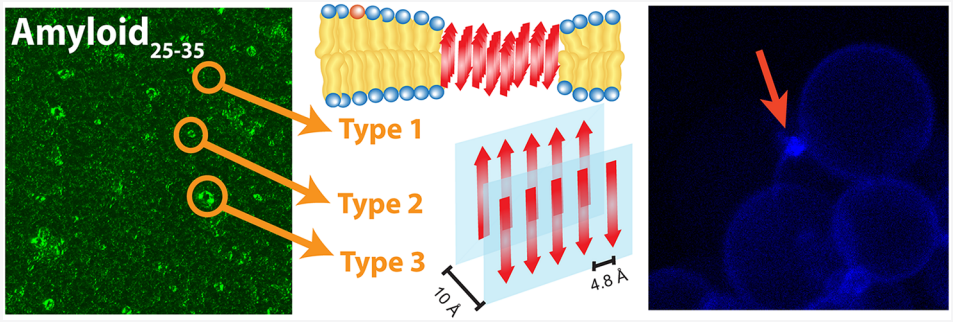

ABSTRACT: Amyloid-β (Aβ) peptides spontaneously aggregate into β- and cross-β-sheets in model brain membranes. These nanometer sized can fuse into larger micrometer sized clusters and become extracellular and serve as nuclei for further plaque and fibril growth. Curcumin and homotaurine represent two different types of Aβ aggregation inhibitors. While homotaurine is a peptic antiaggregant that binds to amyloid peptides, curcumin is a nonpeptic molecule that can inhibit aggregation by changing membrane properties. By using optical and fluorescent microscopy, X-ray diffraction, and UV−vis spectroscopy, we study the effect of curcumin and homotaurine on Aβ_{25-35} aggregates in synthetic brain membranes. Both molecules partition spontaneously and uniformly in membranes and do not lead to observable membrane defects or disruption in our experiments. Both curcumin and homotaurine were found to significantly reduce the number of small, nanoscopic Aβ aggregates and the corresponding β- and cross-β-sheet signals. While a number of research projects focus on potential drug candidates that target Aβ peptides directly, membrane-lipid therapy explores membrane-mediated pathways to suppress peptide aggregation. Based on the results obtained, we conclude that membrane active drugs can be as efficient as peptide targeting drugs in inhibiting amyloid aggregation *in vitro*.

KEYWORDS: *Amyloid-β aggregation, cross-β-sheets, aggregation inhibitor, curcumin, homotaurine, Alzheimer's disease*

INTRODUCTION

More than 150 years ago, extracellular filaments that we now define as amyloids were identified microscopically.[1] Since their discovery, scientists have been trying to understand amyloid structure, how they develop, and ways to inhibit plaque formation. During the 1980s, Glenner and Wong purified cerebrovascular amyloid deposits obtained from Alzheimer's Disease (AD) patients and partially sequenced the 4 kDa subunit protein, which is now known as amyloid-β (Aβ).[2,3] Around the same time, amyloid plaques were isolated from post-mortem brain tissues from AD patients as well as Down syndrome patients with impaired cognition.[4]

The presence of extracellular amyloid-β deposition as neuritic plaques and intracellular accumulation of hyperphosphorylated τ as neurofibrillary tangles remains the primary neuropathologic criteria for AD diagnosis. Hardy and Higgins proposed the amyloid cascade hypothesis in 1992, positing that deposition of Aβ in the brain is the initiating step of AD pathogenesis, leading to subsequent τ deposition, neuron and synaptic loss, and cognitive decline.[5] However, recent studies pointed out pathological roles for other critical cellular and molecular processes.[6] Aβ plaque load in human brains was found not to correlate with the level of cognitive impairment, and dementia was found to precede plaque deposition in animal models. This strongly indicated that Aβ plaques may be the result and not the cause of the neurotoxicity and that smaller soluble protein aggregates and their interactions are likely the drivers of pathology propagation.[7] The extracellular

Received: January 29, 2021
Accepted: March 26, 2021
Published: April 7, 2021

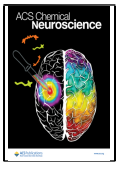

https://doi.org/10.1021/acschemneuro.1c00057
ACS Chem. Neurosci. 2021, 12, 1395−1405

accumulation of Aβ fibrils is not intrinsically cytotoxic, and Aβ does not induce τ accumulation. Amyloid imaging made it possible to observe Aβ accumulation in patients' brains. As a result, it has been found that there are many normal patients with amyloid deposits and also AD patients with very few amyloid deposits.[8] Current disease models suggest that Aβ, either as plaques or as nonfibrillar, soluble oligomeric forms, initiates a pathophysiological cascade leading to τ misfolding and assembly that spreads throughout the cortex, ultimately resulting in neural system failure, neurodegeneration, and cognitive decline.[9] While the genetic evidence strongly supports the importance of Aβ aggregation in instigating the AD cascade, it seems clear that Aβ is necessary but not sufficient and that there are other downstream factors that play a key role. A recent study suggests that regional amyloid deposition does correlate with distant regional hypometabolism, suggesting that amyloid reduces the metabolic activity of distant neurons projecting to regions of amyloid deposition.[10]

In healthy individuals, the amyloid precursor protein (APP) is an integral membrane protein, which is thought to be necessary for synapse formation. The 42-residue transmembrane fragment of APP, which spans the external leaflet of the membrane, is called Aβ. APP is cleaved to release both cytoplasmic and extracellular domains, which harbor both intracellular and extracellular function. However, the improper cleavage of the protein leads to the release of an elongated cytoplasmic domain and a truncated intermembrane domain. This intermembrane domain undergoes further proteolysis to produce $A\beta_{1-42}$. The predominant Aβ species formed from improper cleavage are $A\beta_{1-40}$ and $A\beta_{1-42}$, both of which contain the transmembrane $A\beta_{25-35}$ domain.[11−15]

This short transmembrane segment is commonly used in the study of peptide interactions and partitioning in membranes[11,12,16] and shows neurotoxic properties[17−22] including a high tendency for aggregation and fibrillation.[23−25] β-sheets are easily formed from hydrogen bonding between amide residues from neighboring peptides. The formation of these lateral hydrogen bonds can be accelerated by the stability of the water−hydrophobic interface provided by the cell membrane. It was also suggested that the antiparallel β-sheets are zipped together by adjacent π-bonding between adjacent phenylalanine rings and salt-bridges between charge pairs (glutamate-lysine).[26−28]

Peptidic aggregation inhibitors with known Aβ activity include homotaurine,[29,30] memantine hydrochloride, rivastigmine tartrate, L-phosphoserine,[31] and SG1.[32] These peptic antiaggregants bind to the amyloid peptides and are speculated to prevent the transition from an α-helical structure into the pathological β-sheet structure, thereby suppressing amyloid-fibril formation. A second group of molecules are nonpeptic small-molecule antiaggregants, which interact with membranes and change membrane properties. The list of those molecules includes common drugs and food additives, such as β-carotene, resveratrol, aspirin, green tea extract, curcumin, melatonin, cholesterol, nicotine, and vitamin E.[28,33,34] Evidence was presented that curcumin, for instance, can change size and volume fraction of Aβ clusters by decreasing the hydrophobic mismatch between lipid and peptide domains in membranes.[35] In this paper, we compare the efficacy of homotaurine, a representative of the peptidic aggregation inhibitors, and curcumin, representing a nonpeptic small-molecule antiaggregant, to inhibit $A\beta_{25-35}$ aggregation in model brain membranes.

Homotaurine, also known as tramiprosate or 3-amino-1-propanesulfonic acid or Alzhemed™, is a structural analog and a functional agonist of the neurotransmitter γ-amino butyric acid (GABA) and binds to Lys16, Lys28, and Asp23 of $A\beta_{1-42}$.[29,36] Using electrospray ionization mass spectrometry, Martineau et al. have shown that homotaurine binds to the Aβ peptides through the sulfonate headgroup of the molecule.[37] Homotaurine is able to cross the blood−brain barrier (BBB) and significantly reduce amyloid plaque load in a mouse model of AD.[29] In a Phase II clinical trial of 58 mild-to-moderate AD patients, homotaurine reduced cerebrospinal fluid $A\beta_{1-42}$. Additionally, patients reported no severe side effects with the treatment.[38] Five years after this study was published, a larger clinical study reported similar findings. The posthoc analysis of 790 individuals who completed the 78 week trial showed that homotaurine significantly reduced the loss in hippocampus volume.[39]

Curcumin is the active ingredient of turmeric, a spice frequently used in Asian cuisine, as well as traditional Ayurvedic medicine. Recent epidemiological studies have highlighted its therapeutic potential. Ganguli et al. found that Indians who regularly consumed curcumin, as a part of curry, have a lower rate of AD in comparison with that of the US population.[40] In 2003, Ng and colleagues found that, among a sample of 1010 nondemented elderly participants, those who frequently consumed curcumin performed better in cognitive tests.[41] The interesting correlations from these observational studies led researchers to question if there is a causal relationship between curcumin consumption and improved cognition. Several *in vitro* studies demonstrated the protective effects of curcumin on brain tissues. When Park and colleagues exposed neuronlike PC12 cells to $A\beta_{25-35}$ for 24 h, there was a significant increase in intracellular calcium levels, τ phosphorylation, and DNA damage. Pretreating the cells with curcumin reversed the toxic effect of Aβ.[42] Other studies have shown that curcumin reduced fibril formation in a dose-dependent manner.[43−45] Curcumin is known to be membrane active[46] and it was suggested that its effect on amyloid aggregation is based on membrane thinning and softening, reducing mismatch energy between membrane and protein domains.[35] The *in vivo* studies have also shown promising results. In rat models, curcumin ameliorated cognitive deficits induced by $A\beta_{1-42}$.[47] As for the potential for treating human diseases, Zhang et al. reported that curcumin enhanced Aβ clearance by macrophages of AD patients.[48]

Model brain membranes were made of unsaturated POPC lipids with small amounts of charged DMPS. Amyloid peptides form small, nanometer sized peptide clusters at peptide concentrations of more than 10 mol % in these synthetic, brain-mimicking membranes.[49] The peptides in these clusters show the characteristic diffraction pattern of cross-β-sheets found in amyloid plaques and have been speculated to be the nuclei for extracellular plaque growth.[50] As such, these nanoscopic aggregates represent the earliest stages in the amyloid cascade, and suppressing their formation could inhibit pathological events downstream. Curcumin and homotaurine represent two different types of Aβ aggregation inhibitors. While homotaurine is a peptic antiaggregant that binds to amyloid peptides, curcumin is a nonpeptic molecule that can inhibit aggregation by changing membrane properties. We studied the effect of these two molecules on the aggregation of the membrane active amyloid fragment $A\beta_{25-35}$. Peptide aggregation was visually inspected using microscopical

https://doi.org/10.1021/acschemneuro.1c00057
ACS Chem. Neurosci. 2021, 12, 1395−1405

techniques. In addition, β-sheet and cross-β-sheet signals from peptides in the aggregates were studied by X-ray diffraction and UV−vis spectrometry.

RESULTS AND DISCUSSION

Microscopy. Figure 1 shows bright field and fluorescent microscopy images of all membrane complexes. The pure POPC/DMPS membranes showed a smooth surface and exhibited little to no fluorescence (Figure 1a). The addition of curcumin in Figure 1b led to an even smoother surface and a fluorescent signal, which was uniformly distributed across the membrane indicative of a homogenous distribution of curcumin in the POPC/DMPS bilayers. Also the addition of homotaurine in Figure 1c led to the formation of smooth membrane surfaces and the uniform fluorescence points to a equal distribution of homotaurine in the bilayers. The addition of 20 mol % Aβ_{25-35} to the membranes led to the formation of peptide aggregates in Figure 1d. Aggregates of different sizes are observed in the bright field image, whose peptidic character is clearly identified in the fluorescent images because of their green autofluorescence.

When adding 5 mol % curcumin to the aggregates in Figure 1e, the number of peptide clusters was found to decrease. In particular the number of smaller clusters decreased, as will be discussed in more detail below. The addition of 5 mol % homotaurine (in Figure 1f) was found to result in more aggregates in the bright field and fluorescent images.

We note that the image in the presence of curcumin in Figure 1e appears to be slightly "unfocused" when compared to the other fluorescent images. While the image was recorded as a three-dimensional image with the identical spatial resolution as the other images, the autofluorescence of the curcumin molecules, which also led to additional signals in the UV−vis experiments further below, led to additional fluorescence. As the autofluorescence of curcumin could potentially affect the cluster analysis, cluster number and size was analyzed using the bright field microscopic images.

It was reported that larger peptide aggregates form through fusion of small, nanometer sized peptide clusters. Nanoclusters with typical sizes of 74 nm[35] spontaneously form inside of membranes and are drawn toward each other likely through elastic membrane distortion caused by mismatch between the different domains.[49,51,52] Large aggregates of up to 110 μm have been observed. As shown in Figure 2a, the aggregates in the microscopy images in Figure 1 can be categorized into three types based on their size. The images provide evidence for small aggregates with sizes of less than the resolution of the microscope of ~1 μm (Type 1). These small, nanoscopic aggregates can fuse into larger clusters with typical sizes in the order of 50 μm (labeled Type 2). There is also evidence for large clusters with diameters of about 100 μm (Type 3).

The number of small aggregates was determined using ImageJ scripts. Briefly, binary images were generated from the recorded images by thresholding. The ImageJ function "Analyze Particles" was then used to measure and count objects in the binary images by scanning the image until it finds the edge of an object. The object was then outlined using the wand tool and measured using the "`Measure`" command. The object was then filled to render it invisible, and scanning was resumed until the end of the image was reached. The result is a spreadsheet with the corresponding cluster size distribution. This procedure worked well and was used for the small clusters (Type 1). Large clusters were not reliably detected by this technique, likely because of their sometimes slightly irregular shape. Larger clusters (Type 2 and Type 3)

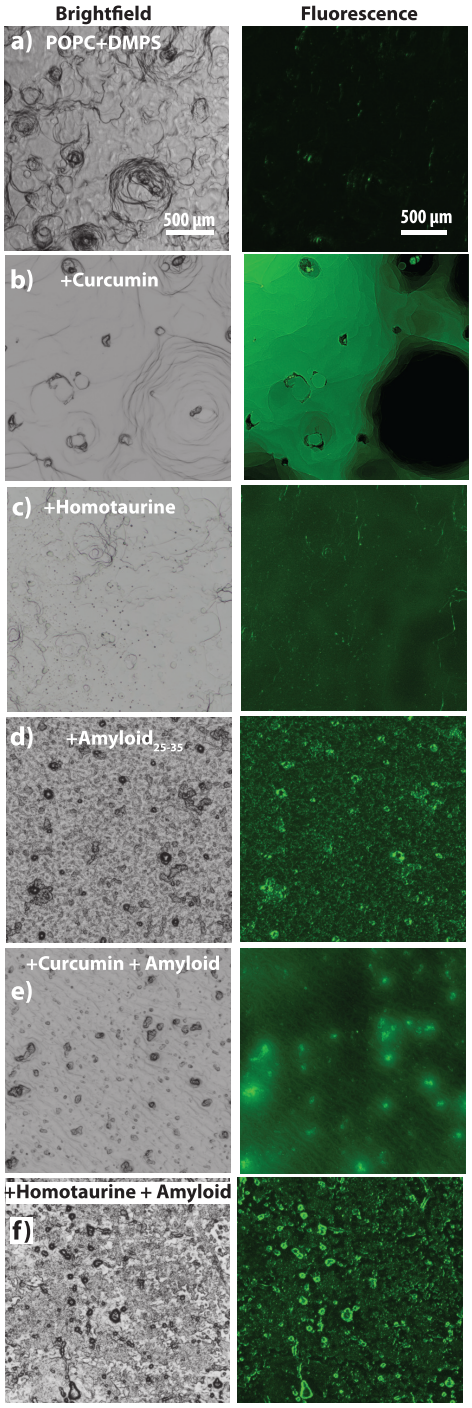

Figure 1. Microscope images of solid supported membrane complexes. Bright field images are shown in the left, and fluorescent images are shown in the right column. (a) Smooth surfaces were observed for pure POPC/DMPS membranes with no fluorescent signal. The incorporation of (b) curcumin and (c) homotaurine did not lead to defects or disrupt the membrane phase. The uniform fluorescence is indicative that the molecules distribute uniformly. (d) Addition of Aβ_{25-35} led to the formation of peptide aggregates. (e) The addition of curcumin significantly reduced the number of small aggregates and also slightly reduced the number of large aggregates. (f) Homotaurine also significantly reduced small aggregates; however, this led to an increase in larger aggregates.

https://doi.org/10.1021/acschemneuro.1c00057
ACS Chem. Neurosci. 2021, 12, 1395−1405

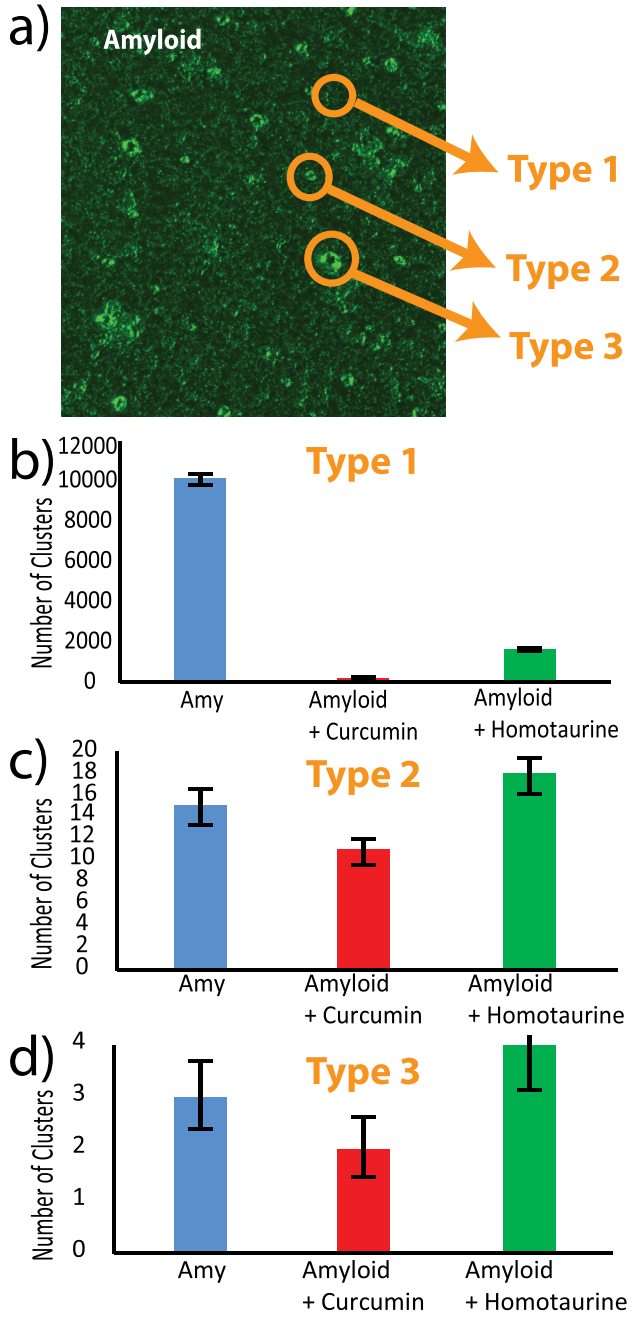

Figure 2. By evaluating the images in Figure 1, the peptide clusters can be divided in three different classes. (a) Type 1 aggregates are smaller than the resolution of the microscope and likely correspond to the nanometer sized (~74 nm) amyloid clusters reported in.[35] Type 2 aggregates are larger, ~50 μm in size. There is also evidence for very large aggregates of about 100 μm, labeled as Type 3. (b–d) All microscope images were analyzed using ImageJ, and the number of aggregates in the different domains for POPC/DMPS + Aβ_{25-35}, +curcumin, and +homotaurine are shown. Following this analysis, curcumin and homotaurine both significantly reduced the size of small Type 1 clusters. While curcumin further reduced the number of Type 2 and Type 3 clusters, homotaurine led to an increase in occurrence of these larger β-sheet aggregates.

were, therefore, measured manually using the measurement tool in the Nikon software, and their number and diameter were recorded. This manual approach was possible, because the number of large clusters was significantly smaller than the number of nanoscopic clusters (10 000 vs ~20).

The results are shown in Figures 2b–d. Following this analysis, both curcumin and homotaurine drastically reduced the number of small, Type 1 aggregates, from 10 139 to 231 and 1627, respectively. While curcumin further reduced Type 2 (15 to 11) and Type 3 aggregates (from 3 to 2), homotaurine was found to increase the count of these larger aggregates (Type 2 from 15 to 18 and Type 3 from 3 to 4).

Confocal images are shown in Figure 3. The membrane (stained with Texas red) fluoresces in red, while the ThT makes β-sheet fluoresce in blue. The first column shows the complete images, while the second and third column show the red (membranes) and blue (β-sheet) channels, respectively. The membrane channel in Figure 3a shows that uniform, defect free GUVs form using this technique. Aβ peptides forming β-sheets (peptide aggregates) are observed in the blue channel. While small β-aggregates (Type 1 aggregates) appear to be uniformly distributed in the membranes of the GUVs, large extracellular clusters (Type 2 or Type 3) can be observed, as marked by the arrow. Uniform GUVs are observed in the presence of homotaurine; however, the intensity of the β-sheet signal in the membranes in the blue channel is reduced, in agreement with the results from epifluorescent microscopy on solid supported membranes. Curcumin, on the other hand, led to an increase of the intensity in the blue channel. This is not related to an increase in the β-sheet signal but due to curcumin's fluorescent properties. Curcumin's absorption was measured to 430 nm (as will be shown below), while curcumin also emits at ~480 nm, in the blue channel.

X-ray Diffraction. The result of the X-ray measurements are two-dimensional diffraction maps for all compounds, which cover the signals of the membranes and the Aβ peptides, as shown in Figures 4a–c. Initial powder scattering of Aβ showed two diffuse bands in resultant reciprocal space corresponding to distances of 4.8 and 10 Å, respectively. Such signals agree with a pattern of β-strands running in-register to one another, as shown in Figure 4d. The X-ray diffraction pattern of cross-β-sheets consists of two signals. The first peak, corresponding to a length scale of 10 Å, represents the interactions that happen between β-sheets and are indicative of cross-β-sheets. The length scale of 4.8 Å represents the interactions within a single β-sheet. The X-ray experiments, therefore, provide two signals: one from the presence of β-sheets and a second one when these β-sheets organize into oligomers made of cross-β-sheets. Additional signals (in the left bottom corner, at small $q_{\|}$- and q_z-values) occur in the two-dimensional data related to the lamellar stacking of the bilayers in the z-direction. The packing of the acyl-tails in the hydrophobic membrane core leads to an in-plane signal at about 4.6 Å ($q_{\|}$ = 1.5 Å^{-1}), as described, for instance, in ref 53. Membrane hydration water leads to a signal at ~1.85 Å^{-1}.[54,55] As reported before,[28,35,49] the integrated intensities of the signals are a direct measure of the volume fraction of the corresponding structures. The two-dimensional data were integrated into line scans, and the insets of Figures 4a–c show fits including the different signals.

The integrated intensities of the β-sheet and cross-β-sheet signals were determined from the fitted height and width of Gaussian peaks and are plotted in Figure 4e. Error bars were determined from the fitted errors using error propagation. As expected from visual inspection of the two-dimensional data, the presence of curcumin and homotaurine reduced the amount of peptides in β-sheets and cross-β-sheets. While curcumin reduced the volume fraction of β-sheets by ~20%, homotaurine led to a ~80% decrease. The cross-β-sheet signal

https://doi.org/10.1021/acschemneuro.1c00057
ACS Chem. Neurosci. 2021, 12, 1395–1405

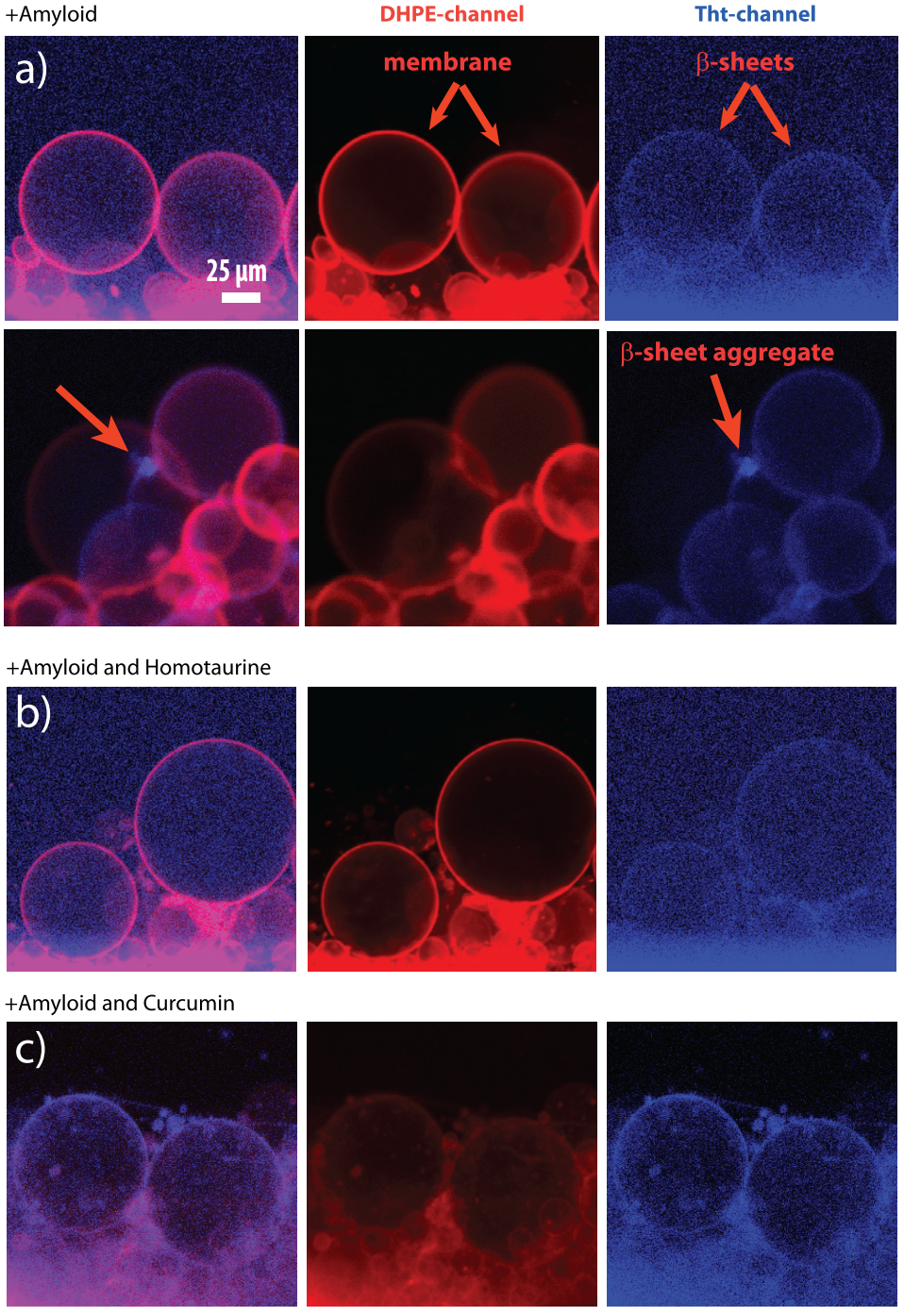

Figure 3. (a) Confocal microscope images of POPC/DMPS liposomes containing 20 mol % Aβ_{25-35}. While the membrane shows up in red in the DHPE channel, the ThT signal related to the formation of β-sheets is observed in blue. Uniform spherical liposomes of about 60 μm were observed. The ThT signal in the membrane is related to small, membrane embedded peptide aggregates below the resolution limit of the microscope (Type 1 aggregates). The images also provide evidence for larger (Type 2 or Type 3) extracellular aggregates, as marked by the arrow. These aggregates are only observed in the blue channel, indicating that they are composed of Aβ peptides in β-sheets. (b) The addition of homotaurine to the liposome solution led to a significant reduction of the ThT signal in the membranes of the liposomes, in agreement with the significant decrease in Type 1 aggregates, in agreement with the epifluorescent microscopy results in Figure 1. (c) Curcumin led to a significant overall increase of the signal in the blue channel because of its fluorescent properties.

was reduced by ~40% (curcumin) and ~90% (homotaurine), respectively. So while homotaurine was found to equally well reduce β- and cross-β-sheets, curcumin reduced the cross-β signal twice as well as the β-sheet signal.

UV−vis Spectroscopy. UV−vis measurements were conducted using liposomes made of POPC/DMPS containing 20 mol % Aβ_{25-35}. Curcumin and homotaurine were then added to the liposome solution and incubated at 37 °C for 2 h before the measurements. The Thioflavin T fluorescence (ThT) assay is frequently used for the detection of amyloid-β.[56] ThT is a β-sheet ligand which binds to amyloid fibrils such that their long axes are parallel, running along the length of the β-sheet.[57] The corresponding spectra for all compounds in

https://doi.org/10.1021/acschemneuro.1c00057
ACS Chem. Neurosci. 2021, 12, 1395−1405

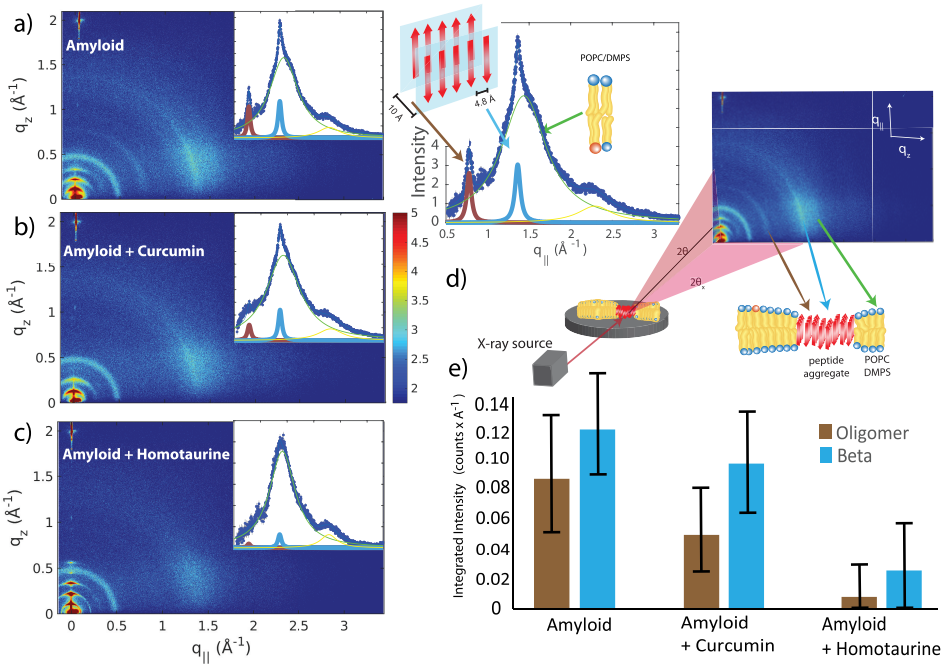

Figure 4. Two-dimensional diffraction maps of POPC/DMPS + Aβ_{25-35} (a) and after the addition of curcumin (b) and homotaurine (c). Experiments were done using solid supported membranes (d). Signals associated with lipids, hydration water, and peptide β- and cross-β-sheets were observed. The two-dimensional data were converted into line scans, shown in the insets, to fit the different contributions. Integrated intensities, which are proportional to the volume fraction of β-sheets and cross-β-sheets (oligomers) (e). Both curcumin and homotaurine led to a decrease of peptides in β- and cross-β-sheets. The effect was more pronounced in membranes containing homotaurine.

Figure 5 show a peak in absorbance at about 410 nm, characteristic of β-sheets.

Data are shown in Figure 5a. While complete UV spectra from 200 to 900 nm were measured, only the region of interest is shown. All measurements were normalized, and the ThT signal was isolated by blank and background subtraction, as described in the Materials and Methods section. The raw data shown in the inset shows curcumin's absorption at 430 nm. This spectrum was fitted by two Gaussian peaks and curcumin's contribution subtracted to get the pure ThT signal. The corresponding integrated signal intensities were calculated and are shown in Figure 5b. The error in the UV data treatment, as determined from the standard deviation in normalizing and averaging 10 measurements, was small for all samples, about 0.02 in absorbance. The error in the curcumin data, however, was larger, as the curcumin signal was subtracted from the data after a fitting procedure. The uncertainty in determining the ThT peak from fitting the data in Matlab was determined to be 0.33, such that the total uncertainty for the curcumin absorbance resulted in 0.35 (in absorbance).

While there was pronounced absorbance in liposomes containing 20 mol % Aβ_{25-35}, the β-sheet signal was reduced by ~60% after the addition of curcumin and homotaurine to the liposome solution, indicating a decrease of peptides in β-sheet structures.

Implications. Many neurodegenerative diseases are associated with lipid alterations.[58−60] The biophysical properties of membranes influence membrane functions, as well as the activity of essential proteins that regulate our cells and lipid bilayer structure and dynamics are essential contributors to membrane functionality.[61−63] Subtle modifications to the structure of membranes are of vital importance to maintain homeostasis. However, the majority of drugs targeting membranes is designed to interact with membrane receptors or enzymes. There has been a shift in recent years to molecules specifically targeting membrane lipids.[63] The field of this so-called membrane-lipid therapy uses membrane-active pharmacology to develop treatments based on the regulation of membrane-lipid composition and membrane structure. While low concentrations of high-affinity drugs are sufficient to disrupt receptors, larger drug concentrations are typically required to change membrane properties sufficiently to affect membranes and membrane protein function.[64−66]

Small, nanometer sized aggregates of Aβ_{25-35} spontaneously form in synthetic brain membranes. These small aggregates can fuse into larger, micrometer sized aggregates which are expelled from the membranes and become extracellular. The peptides in these aggregates show β-sheet and cross-β-sheet signals typically observed in Alzheimer's plaques. This mechanism, therefore, presents a membrane-mediated pathway for the formation of large extracellular amyloid aggregates. In a pathological context, these aggregates may serve as the nuclei for further growth of aggregates or fibrills. The inhibition of formation of these nuclei can thus be an efficient way to inhibit the formation of larger aggregates.

Curcumin and homotaurine represent two different types of Aβ aggregation inhibitors. While homotaurine is a peptic antiaggregant that binds to amyloid peptides, curcumin is a nonpeptic molecule that can inhibit aggregation by changing membrane properties. Both molecules partition spontaneously and uniformly in membranes and do not lead to observable membrane defects or disruption in our experiments.

Both curcumin and homotaurine led to a significant reduction of nanometer sized (Type 1) aggregates in the microscope images. While curcumin also reduced the number

https://doi.org/10.1021/acschemneuro.1c00057
ACS Chem. Neurosci. 2021, 12, 1395−1405

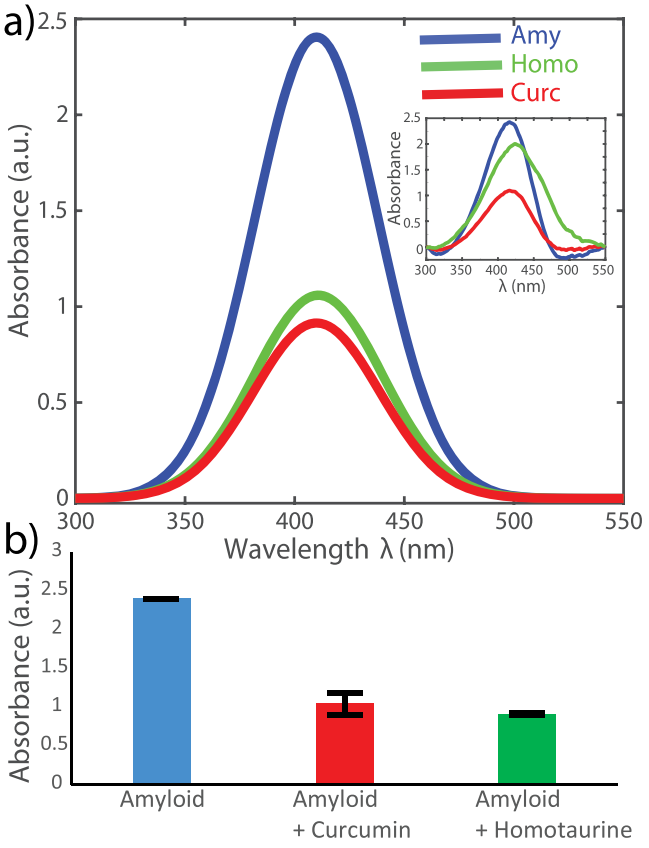

Figure 5. (a) UV−vis absorbance for POPC/DMPS liposomes containing 20 mol % Aβ_{25-35} and after the addition of homotaurine and curcumin. Thioflavin T (ThT) shows absorption around 410 nm in the presence of β-sheets indicating the formation of Aβ aggregates. The spectrum for curcumin was corrected for the absorption of curcumin, as shown in the inset and explained in the main text. (b) Peak absorbance from part (a) as columns including error bars. Absorption was found to reduce by ∼60% when homotaurine and curcumin were added to the liposomes.

of larger clusters (Type 2 and Type 3), homotaurine was found to increase the number of large, extracellular peptide clusters. This finding was further confirmed by the decrease of the β-sheet signal in UV spectroscopy. The X-ray experiments provide two signals: one for the occurrence of β-sheets and a cross-β-sheet signal. Peptides in β-sheets are the basic building blocks of peptide aggregates. These sheets arrange in alternating cross-β-sheets to form larger peptides aggregates. Homotaurine was found to be more efficient in reducing the cross-β signals in the X-ray experiment. The fact that the oligomer signal was more strongly reduced than the β-sheet signal is indicative that the disintegration of aggregates likely occurs by breaking large aggregates into the fundamental, more stable β-sheets before β-sheets dissolve for both drugs. Overall, the findings provide direct experimental evidence that membrane active molecules can have comparable effects on Aβ aggregates as compared to peptide active compounds.

Some comments are in order: The *in vitro* system used in this study is a model system with little physiological relevance or predictive power. The physiological relevance in terms of AD of both curcumin and homotaurine is strongly limited by their bioavailability in the human brain, which is limited by their ability to cross the blood−brain barrier. However, both molecules seem to successfully inhibit the earliest stages of amyloid peptide aggregation, i.e., the formation of nanometer sized aggregates in membranes, which form the nuclei and building blocks of larger aggregates and potentially extracellular fibers later on.[34] As such, they can potentially interrupt the cascade of events that leads to large aggregates of amyloid and τ proteins.

CONCLUSIONS

By combining optical and fluorescent microscopy, X-ray diffraction, and UV−vis spectroscopy, we studied the effect of curcumin and homotaurine on Aβ_{25-35} aggregation in synthetic brain membranes. While homotaurine is a peptic antiaggregant that binds to amyloid peptides, curcumin is a nonpeptic molecule that can inhibit aggregation by changing membrane properties. Both curcumin and homotaurine were found to significantly reduce the number of nanoscopic Aβ aggregates. These small aggregates represent the earliest stages of peptide aggregation and may serve as nuclei for further growth into plaques and fibers. Our results show that *in vitro*, membrane-mediated pathways to suppress peptide aggregation can be as efficient as peptide-based approaches.

MATERIALS AND METHODS

Brain Membrane Mimics Preparation. Synthetic anionic brain membranes were prepared from unsaturated 1-palmitoyl-2-oleoyl-*sn*-glycero-3-phosphocholine (POPC) and saturated, anionic 1,2-dimyristoyl-*sn*-glycero-3-phospho-L-serine (DMPS). All molecules used in this study are depicted in Figure 6. Solutions of POPC and

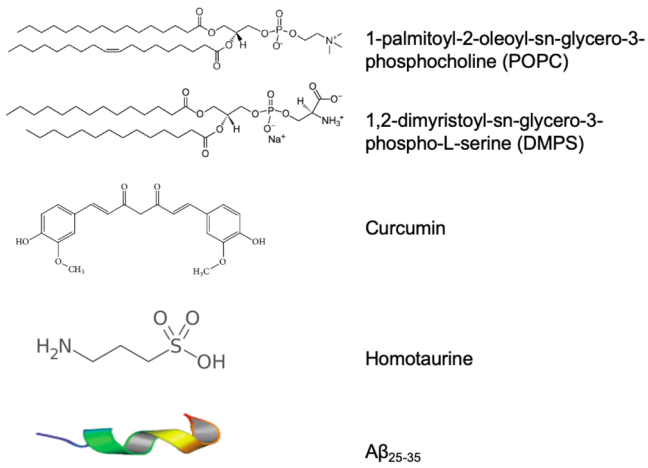

Figure 6. Schematic representation of all compounds used in this study: 1-palmitoyl-2-oleoyl-*sn*-glycero-3-phosphocholine (POPC), 1,2-dimyristoyl-*sn*-glycero-3-phosphoserine (DMPS), curcumin ($C_{21}H_{20}O_6$), homotaurine ($C_3H_9NO_3S$), and amyloid-β_{25--35} ($C_{45}H_{81}N_{13}O_{14}S$).

DMPS at a concentration of 15 mg of lipid per mL of solvent were each dissolved in TFE and chloroform (1:1) and sonicated for 30 min. The amyloid-β peptides were prepared by pretreatment with trifluoroacetic acid (TFA) to disaggregate the peptide, as described in ref 67. This pretreatment included dissolving the peptide in a 1 mg/mL solution of TFA, sonicating with a tip sonicator for four 3 s intervals, and then removing the solvent through evaporation using dry nitrogen gas. The peptides were then redissolved in TFE and chloroform (1:1) at a concentration of 15 mg/mL.[16,35,49,68] The membrane active peptide segment Aβ_{25-35} was added at a peptide concentration of 20 mol % (peptide-to-lipid ratio), which spontaneously forms amyloid aggregates in the membranes.[35,49]

https://doi.org/10.1021/acschemneuro.1c00057
ACS Chem. Neurosci. 2021, 12, 1395−1405

Curcumin and homotaurine were also dissolved in TFE and chloroform (1:1) at concentrations of 15 mg/mL.

Supported Membrane Preparation. Solid supported membranes were prepared for microscopy and X-ray experiments. Membranes were applied onto single-side polished silicon wafers. Silicon wafers (100 mm diameter, 300 μm thick) were precut into 1 × 1 cm^2 chips. The wafers were first pretreated by sonication in dichloromethane at 35 °C for 30 min to remove all organic contamination and leave the substrates in a hydrophobic state. Each wafer was thoroughly rinsed three times by alternating with approximately 50 mL of distilled water and methanol. A heating block was heated to 40 °C; 80 μL of lipid solution was applied on each wafer, and the TFE and chloroform were allowed to slowly evaporate for approximately 10 min. Samples were placed in vacuum for 12 h to remove trace solvents. The bilayers were then incubated and rehydrated in a saturated K_2SO_4 solution overnight at 37 °C, which provides ∼97% relative humidity (RH). This procedure results in highly oriented membrane stacks that uniformly cover the silicon substrates.[16,35,49,68]

Liposome Preparation. Lipid molecules, Aβ_{25-35}, and drug molecules were dissolved in ultrapure (18.2 MΩ cm) water at a concentration of 15 mg/mL for confocal microscopy and UV−vis spectroscopy. Aβ_{25-35} was pretreated with TFA. After removing TFA using nitrogen gas, the peptides were redissolved in ultrapure water at a concentration of 15 mg/mL. When lipids are dissolved in water, they spontaneously form large multilamellar vesicles (MLVs). By sonication of the lipid solution using a tip sonicator (20 times for 5 s each at a power of 100 W), small, unilamellar vesicles (SUVs) are produced. Drug molecules then interact with these SUVs that have typical sizes of ∼200 nm.

Giant unilamellar vesicles (GUVs) with sizes of tens of micrometers (μm) were prepared for confocal laser scanning microscopy by electroformation, as described in ref 69. POPC and DMPS were dissolved in TFE and chloroform (1:1) at a concentration of 10 mg/mL. The lipid molecules were fluorescently labeled with 0.5 mol % Texas Red 1,2-dihexadecanoyl-*sn*-glycero-3-phosphoethanolamine (TR-DHPE). Aβ_{25-35} was pretreated with TFA. After removing TFA using nitrogen gas, the peptides were then redissolved in TFE and chloroform (1:1) at a concentration of 10 mg/mL. Thioflavin T (0.5 mol %) was added to label Aβ peptides in β-sheet configuration. The solutions of POPC, DMPS, Aβ_{25-35}, and labels were mixed and vortexed, and 6 × 3 μL droplets were applied to a platinum wire and dried for 10 min. The wire was then placed in a vacuum for 1 h at room temperature to remove any traces of the solvent. The liposomes were rehydrated, and the plastic rim holding the wire was greased to mount the coverslips. A current of 10 Hz, 3 Vpp, and 1.5 V was applied to the wire for 90 min to grow the liposomes.

Epifluorescent microscopy. Epifluorescent microscopy was conducted using a Nikon Eclipse LV100 ND Microscope. The instrument is equipped with a Plan Fluor BD 10× and 20× objective with numerical apertures of 0.3 and 0.5, respectively. Images were recorded using a Nikon DS-Ri2 Camera with 4908 pixels × 3264 pixels and a pixel-size of 7.3 × 7.3 μm^2. The camera is mounted via a 2.5× telescope to the microscope. This results in a spatial resolution of 0.73 μm/pixel. All images were recorded in episcopic illumination mode using a halogen lamp. Due to a high numerical aperture, the objectives have a small depth of focus, between 0.7 and 0.9 μm.

This setup allows to measure three-dimensional images to determine height profile and topology. The Nikon control software (NIS Elements, Version 4.60.0) was used to record extended depth of focus (EDF) images by combining multiple images with different focal planes. Bright field and fluorescent images were taken for all samples. A B-2A long pass emission filter cube was used with an excitation wavelength of 450−490 nm and a long-pass analyzing filter with a barrier wavelength of 520 nm. Due to their autofluorescence, peptides light up in green in the fluorescent picture. Phospholipids, on the other hand, barely emit a fluorescent signal such that Aβ enriched regions can be identified on the fluorescent image. This technique has been used previously to study Aβ peptide-rich areas in POPC/DMPS bilayers.[49]

Confocal Laser Scanning Microscopy. Liposomes were imaged on a Nikon A1 Confocal Eclipse Ti microscope with Nikon A1plus camera. The microscope was equipped with a Plan Apo 40×/0.9 NA objective lens. Images were recorded using a resolution of 2048 pixels × 2048 pixels, and the recording speed was adjusted to ensure an optimized signal-to-noise ratio for each channel, respectively. Two excitation modes were used: 561 nm (TR-DHPE) and 482 nm (ThT) allowing the identification of the membrane and Aβ peptides in β-sheets, respectively. The instrument was controlled by the Nikon NIS Elements software.

X-ray Diffraction. X-ray diffraction data was obtained using a 9 kW (45 kV, 200 mA) Cu Kα rotating anode at a wavelength of 1.5418 Å using a Rigaku HyPix-3000 2D semiconductor detector with an area of 3000 mm^2 and 100 μm pixel size.[35] Diffraction measurements were conducted under controlled temperature and humidity conditions (30 °C, 98% RH) in a custom-built humidity chamber. The highly oriented membranes were aligned in the diffractometer such that the vertical axis (q_z) in the two-dimensional scans is aligned perpendicular to the membranes and detects structure normal to the bilayers. Molecular structure in the plane of the membranes is detected along the horizontal axis ($q_{\|}$). Several samples were prepared for each compound, and preparation protocols were refined until the experimental results between different samples of the same compound gave not more than 3% deviation in the amplitude, position, and width of the X-ray diffraction peaks.

UV−vis Spectroscopy. UV−vis spectroscopy was conducted using a Nanophotometer (IMPLEN NP80). Liposome samples were used with the addition of trace amounts of Thioflavin T (ThT) to each sample. The ThT assay is commonly used for the detection of amyloid fibrils.[70] The ThT class of molecules has several binding sites and binds to cross-strand ladders that are inherent in repeating side-chain interactions running across the β-strands within a β-sheet layer.[71−73] Thioflavin T is a widely used "gold standard" for selectively staining, visualizing, and quantifying amyloid fibrils. The three classes of binding sites on the Aβ fibrils, BS1, BS2, and BS3, all have high affinities, with BS1 and BS2 also having a high capacity for binding to thioflavin T.[74]

We first prepared liposomes of POPC/DMPS (97:3 mol/mol %) and added 20 mol % Aβ_{25-35} and ThT to form peptide aggregates. Because ThT can accelerate deposition of Aβ peptides,[75] experiments without the presence of compounds were conducted over a period of 24 h to check for aggregation. Samples of Aβ_{25-35} were mixed in a 1.5 mL flask and kept in a shaking incubator at 37 °C. Aliquots were taken and placed in a cuvette at each time point. ThT was then added to the aliquot, and a measurement was conducted. As ThT was found to induce aggregation, which plateaued out after 12 h,[35] all measurements were conducted 12 h after ThT deposition at 30 °C, and all data were normalized to the ThT reference.

Ten measurements (full wavelength scans from 200 to 900 nm) were taken for each sample. A blank was measured before each scan to correct for the effect of cuvette and solvent. The absorbance in each of the 10 measurements was then divided by the total absorbance of the scan to eliminate the effect of potential concentration differences, which is important when working with small sample volumes (1.2 μL). The ten measurements were then averaged, and the UV signal was fitted in Matlab. The ThT and the curcumin signals were well-described by Gaussian peak shapes, and a sloped background was included in the fit and subtracted from the data.

The corresponding spectrum shows absorption at ∼410 nm, characteristic of cross-β-sheets. After a stable fluorescence was reached, appropriate volumes of curcumin and homotaurine were added to the solution. Water was used as a blank, and 10 (1.2 μL) sample measurements were taken for each compound. Complete wave scans were measured and normalized for a wavelength range 200 to 900 nm, and ThT absorption at a wavelength of 410 nm was monitored for each solution.

https://doi.org/10.1021/acschemneuro.1c00057
ACS Chem. Neurosci. 2021, 12, 1395−1405

AUTHOR INFORMATION

Corresponding Author

Maikel C. Rheinstädter − *Department of Physics and Astronomy and Origins Institute, McMaster University, Hamilton, ON L8S 4M1, Canada;* orcid.org/0000-0002-0558-7475; Email: rheinstadter@mcmaster.ca

Authors

Xingyuan Zou − *Department of Physics and Astronomy and Origins Institute, McMaster University, Hamilton, ON L8S 4M1, Canada*

Sebastian Himbert − *Department of Physics and Astronomy and Origins Institute, McMaster University, Hamilton, ON L8S 4M1, Canada*

Alix Dujardin − *Department of Physics and Astronomy, Origins Institute, and Department of Chemistry and Chemical Biology, McMaster University, Hamilton, ON L8S 4M1, Canada*

Janos Juhasz − *Department of Physics and Astronomy, McMaster University, Hamilton, ON L8S 4M1, Canada; Department of Medical Physics, Juravinski Cancer Centre, Hamilton, ON L8V 5C2, Canada*

Samantha Ros − *Department of Chemistry and Chemical Biology, McMaster University, Hamilton, ON L8S 4L8, Canada*

Harald D. H. Stöver − *Department of Chemistry and Chemical Biology, McMaster University, Hamilton, ON L8S 4L8, Canada;* orcid.org/0000-0002-3488-5623

Complete contact information is available at: https://pubs.acs.org/10.1021/acschemneuro.1c00057

Author Contributions

X.Z. conducted research, analyzed data, prepared data for publication, and wrote the paper. S.H. conducted research and provided analysis tools. A.D. contributed figures. J.J., S.R., and H.D.H.S. provided research tools. M.C.R. designed research, conducted research, analyzed data, prepared data for publication, and wrote the paper.

Funding

This research was funded by the Natural Sciences and Engineering Research Council of Canada (NSERC) under RGPIN-2016-06450, the Canada Foundation for Innovation (CFI), and the Ontario Ministry of Economic Development and Innovation. M.C.R. is the recipient of an Early Researcher Award of the Province of Ontario and a University Scholar of McMaster University. The funders had no role in study design, data collection and analysis, decision to publish, or preparation of the manuscript.

Notes

The authors declare no competing financial interest.

The data that support the findings of this study are available from the corresponding author upon reasonable request.

REFERENCES

(1) Haass, C., and Selkoe, D. J. (2007) Soluble protein oligomers in neurodegeneration: lessons from the Alzheimer's amyloid β-peptide. *Nat. Rev. Mol. Cell Biol. 8*, 101−112.

(2) Glenner, G. G., and Wong, C. W. (1984) Alzheimer's disease: initial report of the purification and characterization of a novel cerebrovascular amyloid protein. *Biochem. Biophys. Res. Commun. 120*, 885−890.

(3) Glenner, G. G., and Wong, C. W. (1984) Alzheimer's disease and Down's syndrome: sharing of a unique cerebrovascular amyloid fibril protein. *Biochem. Biophys. Res. Commun. 122*, 1131−1135.

(4) Masters, C. L., Simms, G., Weinman, N. A., Multhaup, G., McDonald, B. L., and Beyreuther, K. (1985) Amyloid plaque core protein in Alzheimer disease and Down syndrome. *Proc. Natl. Acad. Sci. U. S. A. 82*, 4245−4249.

(5) Hardy, J. A., and Higgins, G. A. (1992) Alzheimer's disease: the amyloid cascade hypothesis. *Science 256*, 184−186.

(6) Long, J. M., and Holtzman, D. M. (2019) Alzheimer disease: an update on pathobiology and treatment strategies. *Cell 179*, 312−339.

(7) Bittar, A., Sengupta, U., and Kayed, R. (2018) Prospects for strain-specific immunotherapy in Alzheimer's disease and tauopathies. *NPJ. Vaccines 3*, 1−9.

(8) Kametani, F., and Hasegawa, M. (2018) Reconsideration of amyloid hypothesis and tau hypothesis in Alzheimer's disease. *Front. Neurosci. 12*, 25.

(9) Busche, M. A., and Hyman, B. T. (2020) Synergy between amyloid-β and tau in Alzheimer's disease. *Nat. Neurosci. 23*, 1183−1193.

(10) Pascoal, T. A., Mathotaarachchi, S., Kang, M. S., Mohaddes, S., Shin, M., Park, A. Y., Parent, M. J., Benedet, A. L., Chamoun, M., Therriault, J., et al. (2019) Aβ-induced vulnerability propagates via the brain's default mode network. *Nat. Commun. 10*, 2353.

(11) Dante, S., Hauss, T., and Dencher, N. A. (2002) β-Amyloid 25 to 35 Is Intercalated in Anionic and Zwitterionic Lipid Membranes to Different Extents. *Biophys. J. 83*, 2610−2616.

(12) Dante, S., Hauß, T., and Dencher, N. A. (2006) Cholesterol inhibits the insertion of the Alzheimer's peptide Aβ (25−35) in lipid bilayers. *Eur. Biophys. J. 35*, 523−531.

(13) Haass, C., and Selkoe, D. J. (2007) Soluble protein oligomers in neurodegeneration: lessons from the Alzheimer's amyloid β-peptide. *Nat. Rev. Mol. Cell Biol. 8*, 101−112.

(14) Ladiwala, A. R. A., Litt, J., Kane, R. S., Aucoin, D. S., Smith, S. O., Ranjan, S., Davis, J., Van Nostrand, W. E., and Tessier, P. M. (2012) Conformational differences between two amyloid β oligomers of similar size and dissimilar toxicity. *J. Biol. Chem. 287*, 24765−24773.

(15) Breydo, L., Kurouski, D., Rasool, S., Milton, S., Wu, J. W., Uversky, V. N., Lednev, I. K., and Glabe, C. G. (2016) Structural differences between amyloid beta oligomers. *Biochem. Biophys. Res. Commun. 477*, 700−705.

(16) Dies, H., Toppozini, L., and Rheinstädter, M. C. (2014) The interaction between amyloid-β peptides and anionic lipid membranes containing cholesterol and melatonin. *PLoS One 9*, No. e99124.

(17) Green, P. S., Gridley, K. E., and Simpkins, J. W. (1996) Estradiol protects against β-amyloid (25−35)-induced toxicity in SK-N-SH human neuroblastoma cells. *Neurosci. Lett. 218*, 165−168.

(18) Preston, J. E., Hipkiss, A. R., Himsworth, D. T., Romero, I. A., and Abbott, J. N. (1998) Toxic effects of β-amyloid (25−35) on immortalised rat brain endothelial cell: protection by carnosine, homocarnosine and β-alanine. *Neurosci. Lett. 242*, 105−108.

(19) Dall'Igna, O. P., Fett, P., Gomes, M. W., Souza, D. O., Cunha, R. A., and Lara, D. R. (2007) Caffeine and adenosine A2a receptor antagonists prevent β-amyloid (25−35)-induced cognitive deficits in mice. *Exp. Neurol. 203*, 241−245.

(20) Behl, C., Davis, J., Cole, G. M., and Schubert, D. (1992) Vitamin E protects nerve cells from amyloid βprotein toxicity. *Biochem. Biophys. Res. Commun. 186*, 944−950.

(21) Hensley, K., Carney, J., Mattson, M., Aksenova, M., Harris, M., Wu, J., Floyd, R., and Butterfield, D. (1994) A model for beta-amyloid aggregation and neurotoxicity based on free radical generation by the peptide: relevance to Alzheimer disease. *Proc. Natl. Acad. Sci. U. S. A. 91*, 3270−3274.

(22) Forloni, G., Chiesa, R., Smiroldo, S., Verga, L., Salmona, M., Tagliavini, F., and Angeretti, N. (1993) Apoptosis mediated neurotoxicity induced by chronic application of beta amyloid fragment 25−35. *NeuroReport 4*, 523−526.

(23) Pike, C. J., Burdick, D., Walencewicz, A. J., Glabe, C. G., and Cotman, C. W. (1993) Neurodegeneration induced by beta-amyloid peptides in vitro: the role of peptide assembly state. *J. Neurosci. 13*, 1676−1687.
(24) Hashimoto, M., Shahdat, H. M., Katakura, M., Tanabe, Y., Gamoh, S., Miwa, K., Shimada, T., and Shido, O. (2009) Effects of docosahexaenoic acid on in vitro amyloid beta peptide 25−35 fibrillation. *Biochim. Biophys. Acta, Mol. Cell Biol. Lipids 1791*, 289−296.
(25) Porat, Y., Abramowitz, A., and Gazit, E. (2006) Inhibition of amyloid fibril formation by polyphenols: structural similarity and aromatic interactions as a common inhibition mechanism. *Chem. Biol. Drug Des. 67*, 27−37.
(26) Makin, O. S., and Serpell, L. C. (2005) Structures for amyloid fibrils. *FEBS J. 272*, 5950−5961.
(27) Gazit, E. (2002) A possible role for π-stacking in the self-assembly of amyloid fibrils. *FASEB J. 16*, 77−83.
(28) Khondker, A., Alsop, R. J., and Rheinstädter, M. C. (2017) Membrane-accelerated amyloid-β aggregation and formation of cross-β sheets. *Membranes 7*, 49.
(29) Gervais, F., Paquette, J., Morissette, C., Krzywkowski, P., Yu, M., Azzi, M., Lacombe, D., Kong, X., Aman, A., Laurin, J., et al. (2007) Targeting soluble Aβ peptide with Tramiprosate for the treatment of brain amyloidosis. *Neurobiol. Aging 28*, 537−547.
(30) Kocis, P., Tolar, M., Yu, J., Sinko, W., Ray, S., Blennow, K., Fillit, H., and Hey, J. A. (2017) Elucidating the Aβ42 anti-aggregation mechanism of action of tramiprosate in Alzheimer's disease: integrating molecular analytical methods, pharmacokinetic and clinical data. *CNS Drugs 31*, 495−509.
(31) Meek, A. R., Simms, G. A., and Weaver, D. F. (2013) Searching for an endogenous anti-Alzheimer molecule: identifying small molecules in the brain that slow Alzheimer disease progression by inhibition of β-amyloid aggregation. *J. Psychiatry Neurosci 38*, 269.
(32) Hane, F. T., Lee, B. Y., Petoyan, A., Rauk, A., and Leonenko, Z. (2014) Testing synthetic amyloid-β aggregation inhibitor using single molecule atomic force spectroscopy. *Biosens. Bioelectron. 54*, 492−498.
(33) Carter, M., Simms, G., and Weaver, D. (2010) The development of new therapeutics for Alzheimer's disease. *Clin. Pharmacol. Ther. 88*, 475−486.
(34) Gastaldo, I. P., Himbert, S., Ram, U., and Rheinstädter, M. C. (2020) The Effects of Resveratrol, Caffeine, β-Carotene, and Epigallocatechin Gallate (EGCG) on Amyloid-β25−35 Aggregation in Synthetic Brain Membranes. *Mol. Nutr. Food Res. 64*, 2000632.
(35) Khondker, A., Alsop, R. J., Himbert, S., Tang, J., Shi, A.-C., Hitchcock, A. P., and Rheinstädter, M. C. (2018) Membrane-Modulating Drugs can Affect the Size of Amyloid-β 25−35 Aggregates in Anionic Membranes. *Sci. Rep. 8*, 1−16.
(36) Manzano, S., Agüera, L., Aguilar, M., and Olazarán, J. (2020) A Review on Tramiprosate (Homotaurine) in Alzheimer's Disease and Other Neurocognitive Disorders. *Front Neurol 11*, 614.
(37) Martineau, E., De Guzman, J. M., Rodionova, L., Kong, X., Mayer, P. M., and Aman, A. M. (2010) Investigation of the noncovalent interactions between anti-amyloid agents and amyloid β peptides by ESI-MS. *J. Am. Soc. Mass Spectrom. 21*, 1506−1514.
(38) Aisen, P. S., Saumier, D., Briand, R., Laurin, J., Gervais, F., Tremblay, P., and Garceau, D. (2006) A Phase II study targeting amyloid-β with 3APS in mild-to-moderate Alzheimer disease. *Neurology 67*, 1757−1763.
(39) Aisen, P. S., Gauthier, S., Ferris, S. H., Saumier, D., Haine, D., Garceau, D., Duong, A., Suhy, J., Oh, J., Lau, W. C., Sampalis, J., et al. (2011) Tramiprosate in mild-to-moderate Alzheimer's disease−a randomized, double-blind, placebo-controlled, multi-centre study (the Alphase Study). *Arch. Med. Sci. 7*, 102.
(40) Ganguli, M., Chandra, V., Kamboh, M. I., Johnston, J. M., Dodge, H. H., Thelma, B., Juyal, R. C., Pandav, R., Belle, S. H., and DeKosky, S. T. (2000) Apolipoprotein E polymorphism and Alzheimer disease: the Indo-US cross-national dementia study. *Arch. Neurol. 57*, 824−830.
(41) Ng, T.-P., Chiam, P.-C., Lee, T., Chua, H.-C., Lim, L., and Kua, E.-H. (2006) Curry consumption and cognitive function in the elderly. *Am. J. Epidemiol. 164*, 898−906.
(42) Park, S.-Y., Kim, H.-S., Cho, E.-K., Kwon, B.-Y., Phark, S., Hwang, K.-W., and Sul, D. (2008) Curcumin protected PC12 cells against beta-amyloid-induced toxicity through the inhibition of oxidative damage and tau hyperphosphorylation. *Food Chem. Toxicol. 46*, 2881−2887.
(43) Kim, H., Park, B.-S., Lee, K.-G., Choi, C. Y., Jang, S. S., Kim, Y.-H., and Lee, S.-E. (2005) Effects of naturally occurring compounds on fibril formation and oxidative stress of β-amyloid. *J. Agric. Food Chem. 53*, 8537−8541.
(44) Ono, K., Hasegawa, K., Naiki, H., and Yamada, M. (2004) Curcumin has potent anti-amyloidogenic effects for Alzheimer's β-amyloid fibrils in vitro. *J. Neurosci. Res. 75*, 742−750.
(45) Yang, F., Lim, G. P., Begum, A. N., Ubeda, O. J., Simmons, M. R., Ambegaokar, S. S., Chen, P. P., Kayed, R., Glabe, C. G., Frautschy, S. A., et al. (2005) Curcumin inhibits formation of amyloid β oligomers and fibrils, binds plaques, and reduces amyloid in vivo. *J. Biol. Chem. 280*, 5892−5901.
(46) Alsop, R. J., Dhaliwal, A., and Rheinstädter, M. C. (2017) Curcumin protects membranes through a carpet or insertion model depending on hydration. *Langmuir 33*, 8516−8524.
(47) Zhang, L., Fang, Y., Xu, Y., Lian, Y., Xie, N., Wu, T., Zhang, H., Sun, L., Zhang, R., and Wang, Z. (2015) Curcumin improves amyloid β-peptide (1−42) induced spatial memory deficits through BDNF-ERK signaling pathway. *PLoS One 10*, No. e0131525.
(48) Zhang, L., Fiala, M., Cashman, J., Sayre, J., Espinosa, A., Mahanian, M., Zaghi, J., Badmaev, V., Graves, M. C., Bernard, G., et al. (2006) Curcuminoids enhance amyloid-β uptake by macrophages of Alzheimer's disease patients. *J. Alzheimer's Dis. 10*, 1−7.
(49) Tang, J., Alsop, R. J., Backholm, M., Dies, H., Shi, A.-C., and Rheinstädter, M. C. (2016) Amyloid-β 25−35 peptides aggregate into cross-β sheets in unsaturated anionic lipid membranes at high peptide concentrations. *Soft Matter 12*, 3165−3176.
(50) Eisenberg, D., and Jucker, M. (2012) The amyloid state of proteins in human diseases. *Cell 148*, 1188−1203.
(51) Rheinstädter, M. C., Schmalzl, K., Wood, K., and Strauch, D. (2009) Protein-protein interaction in purple membrane. *Phys. Rev. Lett. 103*, 128104.
(52) Armstrong, C., Sandqvist, E., and C Rheinstädter, M. (2011) Protein-protein interactions in membranes. *Protein Pept. Lett. 18*, 344−353.
(53) Armstrong, C. L., Marquardt, D., Dies, H., Kučerka, N., Yamani, Z., Harroun, T. A., Katsaras, J., Shi, A.-C., and Rheinstädter, M. C. (2013) The observation of highly ordered domains in membranes with cholesterol. *PLoS One 8*, No. e66162.
(54) Rheinstädter, M. C., Seydel, T., Demmel, F., and Salditt, T. (2005) Molecular motions in lipid bilayers studied by the neutron backscattering technique. *Phys. Rev. E 71*, 061908.
(55) Toppozini, L., Armstrong, C. L., Kaye, M. D., Tyagi, M., Jenkins, T., and Rheinstädter, M. C. (2012) Hydration water freezing in single supported lipid bilayers. *ISRN Biophys. 2012*, 1.
(56) Levine, H., III (1993) Thioflavine T interaction with synthetic Alzheimer's disease β-amyloid peptides: Detection of amyloid aggregation in solution. *Protein Sci. 2*, 404−410.
(57) Krebs, M. R., Bromley, E. H., and Donald, A. M. (2005) The binding of thioflavin-T to amyloid fibrils: localisation and implications. *J. Struct. Biol. 149*, 30−37.
(58) Martín, V., Fabelo, N., Santpere, G., Puig, B., Marín, R., Ferrer, I., and Díaz, M. (2010) Lipid alterations in lipid rafts from Alzheimer's disease human brain cortex. *J. Alzheimer's Dis. 19*, 489−502.
(59) Sameni, S., Malacrida, L., Tan, Z., and Digman, M. A. (2018) Alteration in fluidity of cell plasma membrane in Huntington disease revealed by spectral phasor analysis. *Sci. Rep. 8*, 1−10.
(60) Antollini, S. S., and Fabiani, C. (2019) Alzheimer's disease as a membrane disorder: spatial cross-talk among beta-amyloid peptides,

nicotinic acetylcholine receptors and lipid rafts. *Front. Cell. Neurosci. 13*, 309.
(61) Subczynski, W. K., and Wisniewska, A. (2000) Physical properties of lipid bilayer membranes: relevance to membrane biological functions. *Acta Biochim Pol 47*, 613−626.
(62) Escribá, P. V., González-Ros, J. M., Goñi, F. M., Kinnunen, P. K., Vigh, L., Sánchez-Magraner, L., Fernández, A. M., Busquets, X., Horváth, I., and Barceló-Coblijn, G. (2008) Membranes: a meeting point for lipids, proteins and therapies. *J. Cell. Mol. Med. 12*, 829−875.
(63) Phillips, R., Ursell, T., Wiggins, P., and Sens, P. (2009) Emerging roles for lipids in shaping membrane-protein function. *Nature 459*, 379−385.
(64) Herold, K. F., Andersen, O. S., and Hemmings, H. C. (2017) Divergent effects of anesthetics on lipid bilayer properties and sodium channel function. *Eur. Biophys. J. 46*, 617−626.
(65) Zhang, M., Peyear, T., Patmanidis, I., Greathouse, D. V., Marrink, S. J., Andersen, O. S., and Ingólfsson, H. I. (2018) Fluorinated alcohols' effects on lipid bilayer properties. *Biophys. J. 115*, 679−689.
(66) Kapoor, R., Peyear, T. A., Koeppe, R. E., and Andersen, O. S. (2019) Antidepressants are modifiers of lipid bilayer properties. *J. Gen. Physiol. 151*, 342−356.
(67) Jao, S.-C., Ma, K., Talafous, J., Orlando, R., and Zagorski, M. G. (1997) Trifluoroacetic acid pretreatment reproducibly disaggregates the amyloid β-peptide. *Amyloid 4*, 240−252.
(68) Barrett, M. A., Alsop, R. J., Hauß, T., and Rheinstädter, M. C. (2015) The position of Aβ22−40 and Aβ1−42 in anionic lipid membranes containing cholesterol. *Membranes 5*, 824−843.
(69) Juhasz, J., Davis, J. H., and Sharom, F. J. (2012) Fluorescent probe partitioning in GUVs of binary phospholipid mixtures: implications for interpreting phase behavior. *Biochim. Biophys. Acta, Biomembr. 1818*, 19−26.
(70) Hudson, S. A., Ecroyd, H., Kee, T. W., and Carver, J. A. (2009) The thioflavin T fluorescence assay for amyloid fibril detection can be biased by the presence of exogenous compounds. *FEBS J. 276*, 5960−5972.
(71) Biancalana, M., and Koide, S. (2010) Molecular mechanism of Thioflavin-T binding to amyloid fibrils. *Biochim. Biophys. Acta, Proteins Proteomics 1804*, 1405−1412.
(72) Kuznetsova, I. M., Sulatskaya, A. I., Uversky, V. N., and Turoverov, K. K. (2012) Analyzing thioflavin T binding to amyloid fibrils by an equilibrium microdialysis-based technique. *PLoS One 7*, No. e30724.
(73) Lockhart, A., Ye, L., Judd, D. B., Merritt, A. T., Lowe, P. N., Morgenstern, J. L., Hong, G., Gee, A. D., and Brown, J. (2005) Evidence for the presence of three distinct binding sites for the thioflavin T class of Alzheimer's disease PET imaging agents on β-amyloid peptide fibrils. *J. Biol. Chem. 280*, 7677−7684.
(74) Biancalana, M., Makabe, K., Koide, A., and Koide, S. (2009) Molecular mechanism of thioflavin-T binding to the surface of β-rich peptide self-assemblies. *J. Mol. Biol. 385*, 1052−1063.
(75) D'Amico, M., Di Carlo, M. G., Groenning, M., Militello, V., Vetri, V., and Leone, M. (2012) Thioflavin T promotes Aβ (1−40) amyloid fibrils formation. *J. Phys. Chem. Lett. 3*, 1596−1601.

https://doi.org/10.1021/acschemneuro.1c00057
ACS Chem. Neurosci. 2021, 12, 1395−1405